

## PASSIVE TERAHERTZ MICROSCOPY WITH A HIGHLY SENSITIVE DETECTOR

*Yusuke Kajihara*<sup>1,2</sup>, *Takeji Ueda*<sup>1,2</sup>, *Patrick Nickels*<sup>1,2</sup>, *Susumu Komiyama*<sup>1</sup>

<sup>1</sup>Department of Basic Science, The University of Tokyo, Tokyo, Japan, [kaji@thz.c.u-tokyo.ac.jp](mailto:kaji@thz.c.u-tokyo.ac.jp)  
<sup>2</sup>Japan Science and Technology Agency, CREST, Saitama, Japan

**Abstract** – A passive terahertz (THz) microscope has been developed for sensitive imaging of spontaneous THz radiation. The THz microscope consisted mainly of a Ge objective lens, a confocal pinhole, Ge relay lenses, and a highly sensitive THz detector (Charge-Sensitive Infrared Phototransistor, CSIP). Then experimental examinations of the developed microscope were performed. First, THz signals, which were related to the spontaneous thermal radiation, were reasonably obtained. Next a passive THz image was successfully achieved. The lateral resolution of the microscope was derived to be 25  $\mu\text{m}$ , where the depth resolution was derived to be 30  $\mu\text{m}$ . In addition, the lateral resolution was not degraded despite the coverage of GaAs and Si. These results indicate that the THz microscope enables passive imaging with high resolution. This study opens the door to novel THz measurement technology, which can reveal physical and biological phenomena such as molecular motions, biomolecular protein interactions, and semiconductor conditions in their true colors.

**Keywords:** terahertz wave, terahertz detector, passive imaging

### 1. INTRODUCTION

Many photosensitive detectors have been developed in the spectral range from the X-ray to the middle infrared (wavelength  $\lambda$ : 10 pm  $\sim$  10  $\mu\text{m}$ ). They have contributed a great deal to the development of the optical measurement technology. In contrast, only low-sensitivity detectors like bolometers [1] and HgCdTe detectors [2] have been developed in the THz region ( $\lambda$ : 10  $\mu\text{m}$   $\sim$  1 mm). The lack of detectors has restricted the THz measurement technology to small fields such as astronomy and analytical science [3].

Recent technological innovation in semiconductor nanofabrication is now achieving several sensitive THz detectors. For example, a quantum well infrared photodetector (QWIP) with a multiple quantum well [4], a gallium-doped germanium photodetector [5], and a semiconducting tunnel junction detector [6], provide better sensitivity. These detectors are used in various fields including astronomy, military, and security [7]. In addition, THz spectroscopic imaging systems are performed for drug and semiconductor inspection as high-power THz sources are developed [8][9]. These detectors and imaging applications are evolving the THz measurement technology.

However, most of these THz measurements are based on the active method, in which external THz radiation source illuminates a studied object. This active method measures only the object appearance under a situation where the object is measured via reflected or transmitted light. Here, note that all existing objects spontaneously emit THz photons, derived mainly from molecular vibrational-rotation, lattice phonon, and semiconductor impurity levels [10]. If the spontaneous THz photons are passively detected with high throughput and high resolution, it could reveal physical and biological phenomena which remain unknown.

This passive THz detection has been almost impossible because no sufficient-sensitivity detector was developed. Our group, however, has recently developed a much more sensitive THz detector, which was named charge sensitive infrared phototransistor (CSIP) [11]. This detector achieves  $10^2 \sim 10^4$  times as high sensitivity as conventional detectors described above, and the CSIP can detect even single THz photon [12].

Here we plan to achieve the passive THz microscopy with this highly sensitive detector. A few groups have recently performed the passive THz imaging, but their microscopy limited the object temperature to 4.2 K [13] or a low-sensitivity detector (HgCdTe) hindered sufficient throughput [14]. In this study, we design and develop a passive THz microscope with the CSIP. Then we carry out a passive THz imaging of a 300-K object with high throughput. Our future objective is to introduce a near-field optics [15][16][17] to the microscope because diffraction limits the spatial resolution to about half the wavelength [18].

### 2. CHARGE-SENSITIVE INFRARED PHOTOTRANSISTOR

Characteristics of the detector, CSIP, are described below. A schematic diagram and a microscope image of the CSIP are shown in Figs. 1(a) and (b). The CSIP is designed to detect THz photons with wavelengths centered at 14.7  $\mu\text{m}$  (bandwidth: 1  $\mu\text{m}$ ), and is fabricated via standard electron-beam lithography in a GaAs/AlGaAs double quantum well (QW) crystal. The crystal, grown by molecular-beam epitaxy, includes two GaAs QWs separated by a 2-nm thick  $\text{Al}_{0.2}\text{Ga}_{0.8}\text{As}$  tunnel barrier and a 100-nm thick  $\text{Al}_x\text{Ga}_{1-x}\text{As}$  graded barrier layer ( $x=0.01\sim 0.1$ ) as shown in Fig. 1(c).

An electrically isolated plate ( $125 \mu\text{m} \times 125 \mu\text{m}$ ) is formed in the upper QW by electrically biased metal isolation gates (IG). When a THz photon is incident on the isolated upper QW, an electron is excited and tunnels out of the plate. The excited electron, in turn, moves to the lower 2-dimensional electron gas (2DEG) as shown in Fig. 1(d). Missing one electron, the isolated plate is positively charged up, which is sensitively detected as the conductance change in the lower 2DEG layer. This device is thus viewed as a field-effect transistor (FET) with a photosensitive floating gate. The recombination lifetime of the excited hole in the isolated plate is very long, reaching more than an hour. Induced photocurrents are linearly proportional to the intensity of the incident THz radiation. Under constant illumination, the photocurrent is saturated. To avoid this, a brief voltage pulse is applied to a reset gate (RG) to release accumulated positive holes to the source electrode. The QW plate is thereby neutralized, and the phototransistor is reset to the highly sensitive state. The repetition rate of the reset pulse can be higher than 1 KHz, so that the CSIP could allow for high-throughput passive measurement.

The CSIP can be operated well at 4.2 K. Accurate characterization revealed a current responsivity  $R$  of  $4 \times 10^4 \sim 4 \times 10^6$  A/W, a noise equivalent power (NEP) of  $6.8 \times 10^{-19}$  W/Hz $^{1/2}$ , and a specific detectivity  $D^*$  of  $1.2 \times 10^{15}$  cm Hz $^{1/2}$  /W [11]. Compared to conventional highly sensitive THz detectors like QWIP [3], our CSIP is featured by higher values of  $R$  and  $D^*$  as well as a simpler device structure. In addition, the intrinsic dynamic range of the CSIP was suggested to reach  $10^{13}$  (approximately attowatts to microwatts). The CSIP is so sensitive as to sense even single THz photon [17].

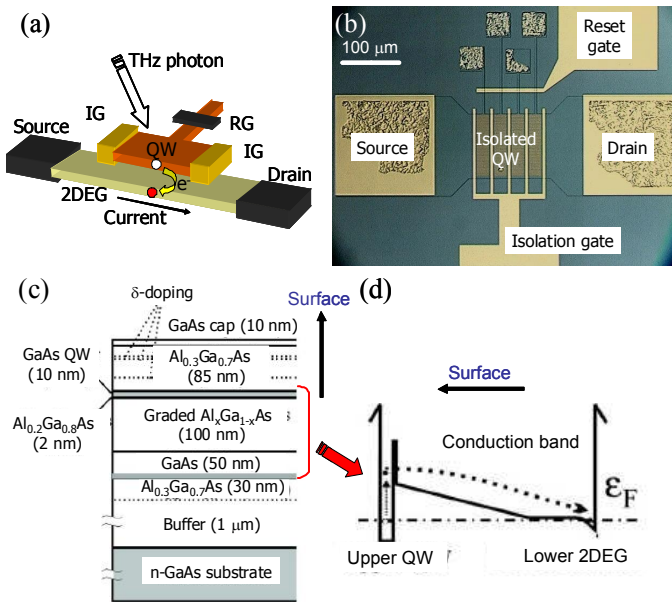


Fig. 1. (a) Schematic diagram of the Charge-Sensitive Infrared Phototransistor (CSIP). (b) Microscope overhead image. (c) Crystal structure grown by molecular-beam epitaxy. (d) Conduction band profile of the double QW crystal; Fermi level  $\epsilon_F$  is indicated as a dot-dash-line. An electron is excited, tunnels out of the upper QW, and finally moves to the lower 2DEG.

### 3. DEVELOPMENT OF A PASSIVE TERAHERTZ MICROSCOPE

#### 3.1. Concept of the passive THz microscope

In order to achieve the passive imaging, a THz microscope should be developed based on the concepts as follows. First, the CSIP must keep low temperature at 4.2 K since the CSIP itself emits THz photons at high temperature. Secondly, the microscope should observe objects placed at room temperature because most challenging objects such as biomolecules and semiconductor devices are expected to be observed at 300 K. Thirdly, high spatial resolution (10- $\mu\text{m}$  order) should be achieved. And finally, it should have the sufficient signal-to-noise ratio (S/N).

#### 3.2. Development of the passive THz microscope

Shown in Fig. 2 is a schematic diagram of a developed passive scanning confocal THz microscope [19]. Fig. 3 shows photographs of the microscope. In Fig. 3, a total image is shown on left side and a closeup near the sample is shown on right side. A sample to be studied at room temperature is placed on a triaxial translation stage controlled stepping motors. The CSIP detector is housed in a metal radiation shield, which is placed in vacuum and thermally anchored to a 4.2 K-cold plate of a liquid helium cryostat. The optical microscopic system consists of a Ge combined objective lens, a ZnSe window, a pinhole, Ge relay lenses, and the CSIP. Spontaneous THz radiation emitted by the sample is collected and focussed on the pinhole by the objective lens, and is finally re-focussed on the CSIP via relay lenses.

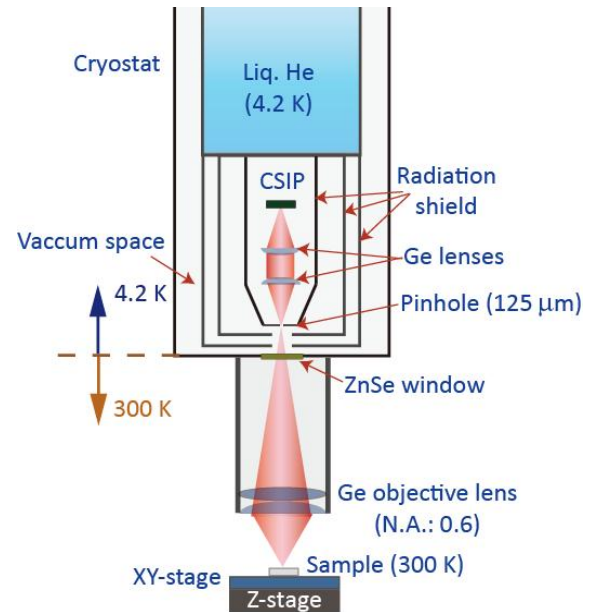


Fig. 2. Schematic diagram of the THz microscope: The CSIP detector is thermally anchored to 4.2 K-cold plate in vacuum, while the sample is placed outside the cryostat. The Ge objective lens has a numerical aperture of 0.60 so as to provide a spatial resolution of  $25 \mu\text{m}$ . The focal depth of the microscope is  $20 \mu\text{m}$ . The diameter of the pinhole is  $125 \mu\text{m}$ , which is equal to the beam waist size.

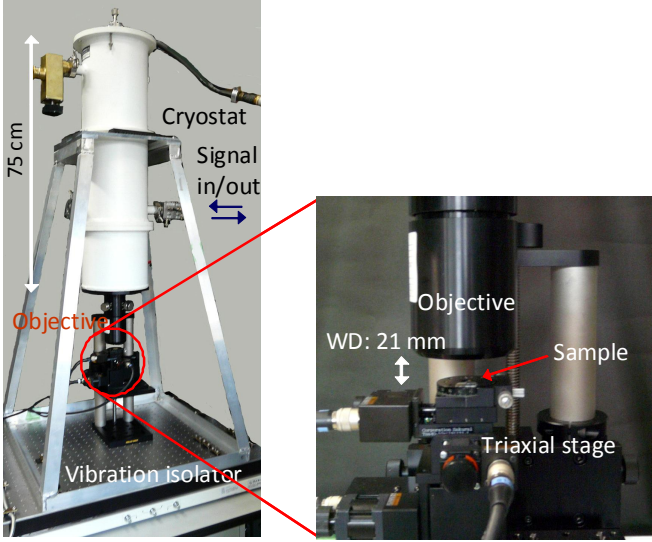


Fig. 3. Photographs of the microscope: (Left) Total image (Right) Closeup near the sample.

The Ge objective lens has a numerical aperture of 0.60 (working distance: 21 mm), so that this optical system provides a spatial resolution of 25  $\mu\text{m}$ . The ZnSe window separates the vacuum space leading to the 4.2 K-region from the external 300 K-environment. The pinhole blocks THz photons entering from places other than the focal point of the sample and also works as a confocal pinhole [20]. The diameter of the pinhole is chosen to be 125  $\mu\text{m}$ , which is equal to the beam waist size. The focal depth of the microscope is 20  $\mu\text{m}$ . The Ge lenses serve also as filters to the unwanted visible/near-infrared radiation. With the pinhole and the Ge lenses, the microscope achieves sufficient S/N. As described above, the THz microscope meets the concepts mentioned before.

## 4. PASSIVE IMAGING

### 4.1. Measurement of THz radiation

We first evaluated the fundamental function of the passive THz microscope by measuring the spontaneous THz radiation. The studied object was a 77 K-glass plate, a 300 K-glass plate, and a soldering-iron tip (oxidized copper) at  $\sim 600$  K. The 77-K glass plate was prepared by placing a 2 mm-thick slide glass in a styrofoam plate filled with liquid nitrogen. (The inside faces of the styrofoam plate were covered by black papers.) When IG and RG are both biased at less than -0.42 V, the upper QW is electrically isolated and the detector starts working. In this experiment, IG and RG were both biased at -0.50 V. During the measurement, reset pulses (+0.30 V-amplitude and a 100 ns-duration) were periodically applied to RG to neutralize the upper QW. The repetition rate of the reset pulse was 500 Hz.

Fig. 4 displays real-time traces of the detector current, which exhibit saw-tooth like waves caused by application of a reset pulse. The lowest, middle, highest curves mean the signals from 77 K-glass plate, a 300 K-glass plate, and a soldering-iron tip, respectively. The gradients of the plots

mean the transition of the photocurrent. We express the THz signal in terms of the peak-to-peak current of each signal in Fig. 4. THz signals can be measured by a lock-in amplifier referenced to the frequency of the reset pulse. We also measured the saturation time of the CSIP by reducing the repetition rate of the reset pulse. The saturation time was 33 Hz (30 ms) when a 300 K-glass plate was placed on the focal position.

Here we wish to check the validity of the experimental results in Fig. 4. Planck's formula for black body radiation provides the radiation intensity  $B(\lambda, T)$  as

$$B(\lambda, T) = \frac{2hc^2}{\lambda^5} \frac{1}{\exp(hc / \lambda k_B T) - 1}, \quad (1)$$

where  $\lambda$  is the wavelength,  $T$  is the temperature,  $h$  is the Planck's constant,  $c$  is the light velocity, and  $k_B$  is the Boltzmann's constant [21]. By assigning  $\lambda = 14.7 \mu\text{m}$ , Eq. 1 derives  $B(\lambda, 77 \text{ K}) = 5.1 \times 10^2 \text{ J/m}^3 \cdot \text{s}$ ,  $B(\lambda, 300 \text{ K}) = 6.9 \times 10^6 \text{ J/m}^3 \cdot \text{s}$ , and  $B(\lambda, 600 \text{ K}) = 4.2 \times 10^7 \text{ J/m}^3 \cdot \text{s}$ . The intensity ratio of thermal radiation is hence derived as  $B(77 \text{ K}) : B(300 \text{ K}) : B(600 \text{ K}) \approx 10^{-4} : 1 : 6$ , which indicates that the radiation intensity of the 77 K-glass is negligibly small (Fig. 5 (a)). Thus, the finite signal of 77-K glass in Fig. 4 is ascribed to the stray light. By expressing the THz signal as  $P$ , we have  $P(77 \text{ K}) : P(300 \text{ K}) : P(600 \text{ K}) = 0.08 \mu\text{A} : 0.14 \mu\text{A} : 0.48 \mu\text{A}$  by Fig. 4. By subtracting the stray light component  $P(77 \text{ K-glass}) = 0.08 \mu\text{A}$ , we derive  $\{P(300 \text{ K-glass}) - (\text{stray light})\} : \{P(600 \text{ K-iron tip}) - (\text{stray light})\} = 0.06 \mu\text{A} : 0.33 \mu\text{A}$ , which approximately agrees to the expectation, 1 : 6, predicted by Planck's formula.

Then we estimate the collection efficiency (Detected photon number / Detectable photon number) from the result of the 300 K-glass. Here the total incident photon flux  $\Phi$  to the detector shown in Fig. 5 (b) is given by

$$\Phi = \varepsilon f_{\text{att}} \left[ \frac{B(\lambda, T) \Omega \Delta \lambda_d}{hc / \lambda} \right] S_{\text{sam}}, \quad (2)$$

where  $\varepsilon \sim 0.85$  is the emissivity of glass,  $f_{\text{att}} \sim 0.49$  is the attenuation due to reflection and absorption at the Ge lenses (0.7) and the ZnSe window (0.7),  $\Omega = 1.77 \text{ sr}$  (given by N. A. = 0.6) is the solid angle,  $\Delta \lambda_d = 1.0 \mu\text{m}$  [12] is the detector bandwidth, and  $S_{\text{sam}}$  is the effective emission area. Effective emission area  $S_{\text{sam}}$  can be derived considering the expected resolution of the microscope (25  $\mu\text{m}$ ). By assigning these values, photon flux  $\Phi$  is estimated to be  $1.9 \times 10^{11}$  photons/s. Detectable photon number is expressed by  $\eta \Phi$ , where  $\eta = 2\%$  [12] is the quantum efficiency of the CSIP detector. Hence  $\eta \Phi$  is derived to be  $3.8 \times 10^9$  photons/s. Here we consider capacitance  $C_{\text{det}}$  between the upper isolated QW and the lower 2DEG. The size of the upper isolated QW is  $125 \mu\text{m} \times 125 \mu\text{m}$  and the distance between the upper QW and the 2DEG is 150 nm. These parameters and the relative permittivity of GaAs = 13.0 derive  $C_{\text{det}}$  to be 12 pF. The hole saturation in upper QW occurs when the capacitance bias is more than 50 mV [18]. Thus, accumulable hole

number of the upper QW is derived to be  $3.7 \times 10^6$ . Here the expected saturation time  $t_s$  is given by (accumulable hole number) /  $(\eta\Phi)$  and  $t_s$  is estimated to be 1.0 ms. Considering the saturation time of the experiment = 30 ms, the collection efficiency is 1.0 ms / 30 ms = 0.033. This value is consistent since  $f_{\text{Au}}$  must be much smaller due to other environmental effects than reflection and absorption.

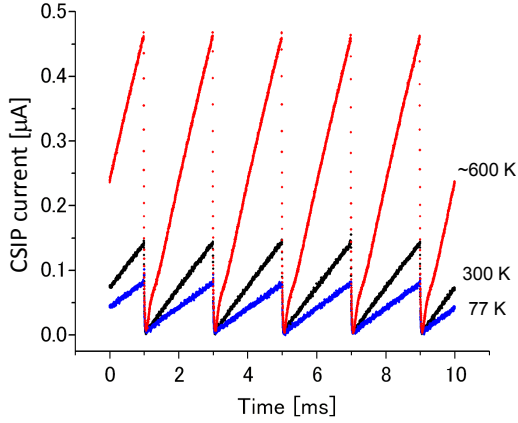


FIG. 4. Real-time traces of the CSIP output current.

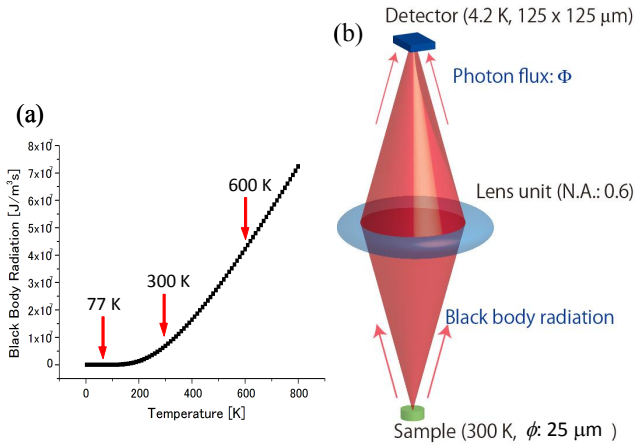


Fig. 5. (a) Black body radiation (wavelength = 14.7  $\mu\text{m}$ ) calculated by Planck's formula. (b) Photon flux to the detector.

#### 4.2. Passive THz imaging

Next we carried out passive THz imaging. A sample to be studied was a CSIP surface placed at room temperature. A microscope image of the studied sample is shown in Fig. 1 (b). On the CSIP surface, Au was evaporated 100-nm thick (electrode of source, drain, isolation gate, and reset gate), the surface of the isolated QW was covered by Au and GaAs, and other surface was covered by GaAs. Prior to the measurements, the height of the sample surface was carefully adjusted to the focal position. A  $500 \mu\text{m} \times 500 \mu\text{m}$  area on the CSIP sample was scanned at a  $10 \mu\text{m}$ -interval with a scan speed of 100 ms/step. This scan speed was limited by the maximum driving speed of the stepping motor stage and the detection speed could be set much faster. THz signals were measured every step by a lock-in amplifier, where the reset repetition rate was 500 Hz and the time constant of the lock-in amplifier was 10 ms.

Fig. 6 displays an obtained passive THz image of the CSIP surface. The materials were clearly distinguished and

the image was almost the same as Fig. 1(d) (left-right reversal). In this image, dark area denotes smaller signal than other areas. As expressed by Eq. (2), photon flux  $\Phi$  depends on emissivity  $\varepsilon$ . By considering  $\varepsilon_{\text{Au}}$  is much smaller than  $\varepsilon_{\text{GaAs}}$  [22], this result is reasonable.

Then the lateral resolution of the THz microscope was estimated from the THz intensity profile along a dot line in Fig. 6, crossing Au electrode, GaAs surface, and Au/GaAs antennas. The scan length was  $600 \mu\text{m}$ , the scan interval was  $1 \mu\text{m}$ , the scan speed was 10 ms/step, the reset repetition rate was 500 Hz, and the lock-in time constant was 10 ms. The curve in Fig. 7 displays the profile. The lateral resolution of the THz microscope was derived to be  $25 \mu\text{m}$  by measuring the edge width between Au and GaAs. The estimated resolution agrees with the designed value, which confirms that the microscope is well-calibrated. We note, in Fig. 7, that the signal-to-noise ratio (S/N) reaches a value higher than  $10^3$  with an averaging time of 10 ms, where the signal implies the amplitude of the saw-tooth wave and the noise is the current fluctuation. The excellent S/N allows for detection of smaller modulation signals, which will make feasible the introduction of near-field optical techniques with higher spatial resolution.

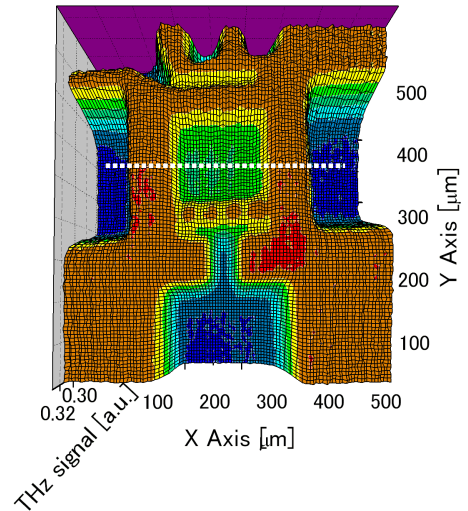


Fig. 6. Passive THz image of the CSIP surface, which is left-right reversal from the actual surface shown in Fig. 1(b).

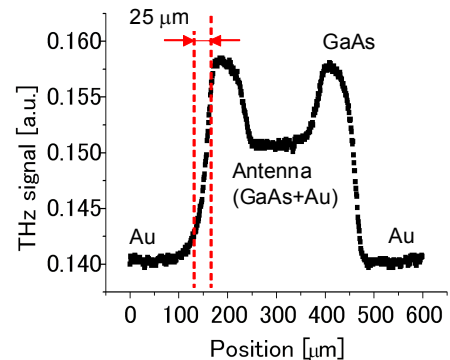


Fig. 7. THz intensity profile along the dot line shown in Fig. 6. The lateral resolution was estimated to be  $25 \mu\text{m}$ .

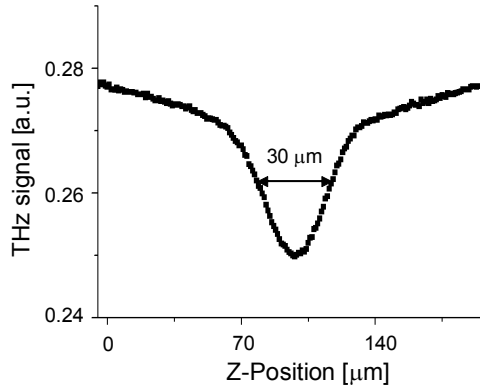


Fig. 8. THz intensity profile along z-axis: The depth resolution of the passive THz microscope was estimated to be 30  $\mu\text{m}$  by measuring the half bandwidth.

We also estimated the depth resolution of the THz microscope, which had the confocal system. An Au area on the studied sample was moved to the focal position and the sample was scanned along z-axis (optical axis). The scan length was 200  $\mu\text{m}$ , the scan interval was 1  $\mu\text{m}$ , the scan speed was 10 ms/step, the reset repetition rate was 500 Hz and the lock-in time constant was 10 ms. The curve in Fig. 8 displays the profile. The THz signal intensity is smallest when the sample (Au) is adjusted to the focal position. By measuring the half bandwidth in Fig. 8, the depth resolution was derived to be 30  $\mu\text{m}$ .

#### 4.3. Imaging a sample covered by GaAs or Si plate

Passive THz images were taken also by entirely covering a sample surface by a 400  $\mu\text{m}$ -thick semi-insulating GaAs plate and by a 400  $\mu\text{m}$ -thick non-doped Si plate. Studied sample was prepared by evaporating Au on a glass plate. The edge between Au and glass on the sample was scanned on the condition that sample surface was covered by GaAs or Si plate. The experimental conditions were the same as the line scan demonstrated in Sec. 4.2. The results are shown in Figs. 9 and 10. Au and glass were clearly distinguished despite the coverage by the GaAs or Si plate, which is transparent in the wavelength range of  $14.7 \pm 0.5 \mu\text{m}$  (transmittivities  $\sim 0.5$  in both materials). The lateral resolution is estimated to be 25  $\mu\text{m}$  in both results and it confirms that the resolution is not degraded despite the coverage of GaAs and Si. It is hence suggested that the passive THz microscope here can be useful for the inspection of semiconductor devices.

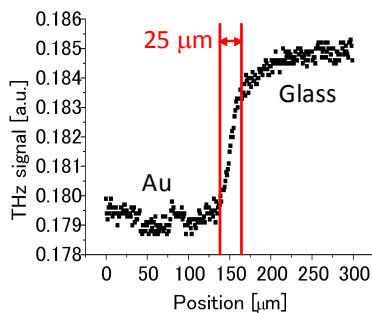


Fig. 9. Result of the line scans along Au-glass edge covered by semi-insulating GaAs plate.

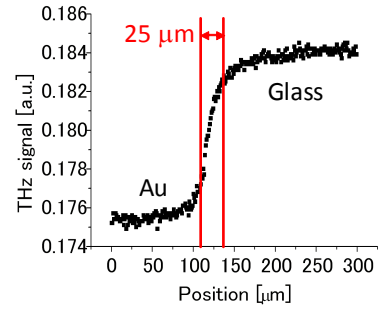


Fig. 10. Result of the line scans along Au-glass edge covered by non-doped Si plate.

## 5. CONCLUSIONS

In this study, passive THz microscopy was demonstrated with the highly sensitive detector, CSIP. The passive THz microscope was developed to observe objects at room temperature with a high spatial resolution and a sufficient S/N. This microscope consisted mainly of the Ge objective lens, the ZnSe window, the confocal pinhole, Ge relay lenses, and the CSIP. Then passive THz measurements were carried out. First, the signals of the spontaneous THz radiation were obtained related to the thermal radiation. Next a two-dimensional passive image was successfully achieved by scanning the CSIP surface. The lateral resolution of the THz microscope was estimated to be 25  $\mu\text{m}$ , where the depth resolution was estimated to be 30  $\mu\text{m}$ . In addition, it was confirmed that the resolution was not degraded despite the coverage of GaAs and Si. These results indicate that the THz passive imaging can be demonstrated with our THz microscope. This passive THz measurement could allow for much further improvement of the measurement technology. Our future work is to introduce the near-field optics to the THz microscope for much further resolution. Establishment of the near-field THz microscopy could promise to realize a novel measurement technology in various fields.

## ACKNOWLEDGMENTS

This work was supported by CREST project of Japan Science and Technology Agency (JST), Grant-in-Aid for Young Scientists (Start-up), Mitutoyo Association for Science and Technology, and the Sumitomo Foundation.

## REFERENCES

- [1] P. L. Richards, "Bolometers for infrared and millimeter waves", *J. Appl. Phys.*, vol. 76, pp. 1-24, Jan. 1994.
- [2] P. Norton, "HgCdTe infrared detectors", *Opto-electron. Rev.*, vol. 10, no. 3, pp. 159-174, Sep. 2002.
- [3] D. T. Phillips and J. Keene, "Submillimeter astronomy", *Proc. IEEE*, vol. 80, no. 11, pp. 1662-1678, Nov. 1992.
- [4] A. Rogalski, "Quantum well photoconductors in infrared detector technology", *J. Appl. Phys.*, vol. 93, no. 8, pp. 4355-4391, April 2003.
- [5] M. Fujiwara, T. Hirao, H. Kawada, H. Shibai, S. Matsuura, H. Kaneda, M. Patrashin, and T. Nakagawa, "Development of a gallium-doped germanium far-infrared photoconductor

- direct hybrid two-dimensional array”, *Appl. Opt.*, vol. 42, no. 12, pp. 2166-2173, April 2003.
- [6] S. Ariyoshi, H. Matuo, C. Otani, H. Sato, H. M. Shimizu, K. Kawase, and T. Noguchi, “Characterization of an STJ-based direct detector of submillimeter waves”, *IEEE Trans. Appl. Supercond.*, vol. 15, pp. 920-923, Feb. 2005.
- [7] D. Mittleman, *Sensing with Terahertz Radiation*, Springer, Berlin, 2003.
- [8] K. Kawase, Y. Ogawa, Y. Watanabe, and H. Inoue, “Non-destructive terahertz imaging of illicit drugs using spectral fingerprints”, *Opt. Express.*, vol. 11, no. 20, pp. 2549-2554, Oct. 2003.
- [9] M. Yamashita, C. Otani, K. Kawase, K. Nikawa, and M. Tonouchi, “Noncontact inspection technique for electrical failures in semiconductor devices using a laser terahertz emission microscope”, *Appl. Phys. Lett.*, vol. 93, no. 4, pp. 041117 1-3, July 2008.
- [10] M. Tonouchi, “Cutting-edge terahertz technology”, *Nature Photonics*, vol. 1, pp. 97-105, Feb. 2007.
- [11] Z. An, J.-C. Chen, T. Ueda, and S. Komiyama, “Infrared phototransistor using capacitively coupled two-dimensional electron gas layers”, *Appl. Phys. Lett.*, vol. 86, pp. 172106 1-3, April 2005.
- [12] T. Ueda, Z. An, K. Hirakawa, and S. Komiyama, “Charge-sensitive infrared phototransistors: Characterization by an all-cryogenic spectrometer”, *J. Appl. Phys.*, vol. 103, pp. 093109 1-7, May 2008.
- [13] K. Ikushima, Y. Yoshimura, T. Hasegawa, S. Komiyama, T. Ueda, and K. Hirakawa, “Photon-counting microscopy of terahertz radiation”, *Appl. Phys. Lett.*, vol. 88, pp. 152110 1-3, April 2006.
- [14] Y. De Wilde, F. Formanek, R. Carminati, B. Gralak, P. Lemoine, K. Joulain, J. Mulet, Y. Chen, and J. Greffet, “Thermal radiation scanning tunneling microscopy”, *Nature (London)*, vol. 444, no. 7, pp. 740-743, Dec. 2006.
- [15] B. Knoll and F. Keilmann, “Near-field probing of vibrational absorption for chemical microscopy”, *Nature (London)*, vol. 399, no. 13, pp. 134-137, May 1999.
- [16] P. C. M. Planken and N. C. J. van del Valk, “Spot-size reduction in terahertz apertureless near-field imaging”, *Opt. Lett.*, vol. 29, no. 19, pp. 2306-2308, Oct. 2004.
- [17] M. Born and E. Wolf, *Principles of Optics, 6th edition*, Pergamon Press, Oxford, 1981.
- [18] Z. An, T. Ueda, S. Komiyama, and K. Hirakawa, “Metastable excited states of closed quantum dot with high sensitivity to infrared photons”, *Phys. Rev. B*, vol. 75, pp. 085417 1-7, Feb. 2005.
- [19] Y. Kajihara, S. Komiyama, P. Nickels, and T. Ueda, “A long-wavelength infrared microscope with a highly sensitive phototransistor”, *Rev. Sci. Instrum.*, vol. 80, no. 6, June 2009 (to be published).
- [20] R. H. Webb, “Confocal optical microscopy”, *Rep. Prog. Phys.*, vol. 59, no. 3, pp. 427-471, March 1996.
- [21] C. Kittel and H. Kroemer, *Thermal Physics 2nd edition*, W. H. Freeman, San Francisco, 1980.
- [22] A. S. Jordan, “Determination of the total emittance on n-type GaAs with application to Czochralski growth”, *J. Appl. Phys.*, vol. 51, no. 4, pp. 2218-2227, Apr. 1980.